

Rigid-Body-Spring Network modeling of cement-based composites

J.E.Bolander & M.Yip

Department of Civil and Environmental Engineering, University of California, Davis, CA, USA

K.Moriizumi

Department of Architecture, Nihon University, Tokyo, Japan

M.Kunieda

Department of Civil Engineering, Gifu University, Gifu, Japan

ABSTRACT: This paper reports on the development of the Rigid-Body-Spring Network (RBSN) approach, which can be categorized as a lattice model, and its application to analyzing quasi-brittle failure of cement-based composites. Attention is first given to elastic stress analysis, which is fundamental to modeling crack initiation and propagation. The potential for modeling crack propagation across random networks is demonstrated through comparisons with theory and mode I fracture test results. Due to the implementation of a crack band model within the RBSN, crack propagation is objective with respect to network component size and geometry. The latter part of the paper presents preliminary efforts toward modeling compressive failure under uniaxial loading, as well as work towards extending the analysis framework to three dimensions.

1 INTRODUCTION

A variety of numerical models based on primitive, discrete structural components (e.g. lattice models) have been used to clarify fracture phenomena within cement-based materials, such as concrete (Schlangen and van Mier, 1992). These studies have provided useful, often realistic, interpretations of fracture, particularly with respect to the mechanisms contributing to tension softening. There is currently a good potential for applying such models to general loading cases, including those leading to compressive failure.

This paper reports on the development of the Rigid-Body-Spring Network (RBSN) approach and its application to analyzing quasi-brittle failure of cement-based composites. After describing the basic concepts of RBSN, attention is given to its abilities for elastic stress analysis, which is fundamental to modeling crack initiation and propagation. Random lattice networks generally exhibit spurious heterogeneity that can overshadow important aspects of material behavior, particularly when modeling fracture in homogeneous materials (or homogeneous phases within composite materials). This issue is resolved through the use of a crack band model for fracture within the RBSN approach. Analyses of concrete

compact tension specimens are conducted to demonstrate model objectivity with respect to size and geometry of the network components. The paper concludes with an analysis of concrete failure in uniaxial compression and preliminary work towards extending the RBSN to a three-dimensional analysis framework.

2 RBSN FORMULATION

The RBSN is based on the Rigid-Body-Spring Model (RBSM) developed by Kawai (1978). In the RBSN approach, the material domain is discretized using a Voronoi diagram on a set of randomly distributed points, or nuclei (Fig. 1): network degrees of freedom are defined at the nuclei. System flexibility is lumped into zero-size spring sets that interconnect the rigid Voronoi cells along their common boundary segments, as shown in Figure 2. Each spring set consists of a normal, tangential, and rotational spring oriented local to the boundary segment.

The RBSN is best categorized as a lattice model, with the Voronoi cell nuclei acting as lattice sites. The basic element of the RBSN can be viewed as a special type of beam-spring element composed of two rigid arms connected by the

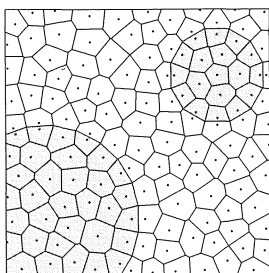


Figure 1. Voronoi discretization of a multi-phase material

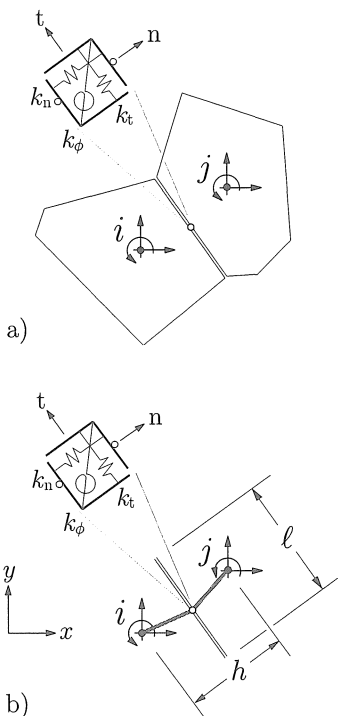


Figure 2. RBSN basic element: a) rigid cell depiction; and b) equivalent beam-spring element

zero-size spring set, as shown in Figure 2b. The distance between the Voronoi cell nuclei, h , and the length of the common boundary segment, l , are used to scale the spring stiffnesses

$$\begin{aligned} k_n &= Etl/h \\ k_t &= Etl/h \\ k_\phi &= k_n l^2/12 \end{aligned} \quad (1)$$

where E is the elastic modulus of the continuum material and t is the specimen thickness. System equilibrium equations are constructed from each elemental unit (i.e. each two-cell subassembly) using the direct stiffness method.

Despite the appearance of a deformed RBSN, contact algorithms are not part of the formulation. In that sense, the RBSN is quite different from approaches such as the Distinct Element Method, Discontinuous Deformation Analysis, and methods for particle dynamics, all of which involve routines to identify current neighbors and contact conditions as the problem topology changes.

3 ELASTIC STRESS ANALYSIS

3.1 Stress retrieval algorithm

The ability to extract accurate stress measures from the network is essential for both analysis and understanding the model behavior. Schlangen (1995) has computed stress measures at the nodal sites of a beam lattice, rather than in the beams themselves. In a similar manner, consider a Voronoi cell subjected to intercell spring forces, F_{ni} and F_{ti} , on each boundary segment i (Fig. 3). These are the forces in the normal and tangential springs shown in Figure 2. Stress is computed by sectioning the Voronoi cell through its nucleus and then invoking force equilibrium on either portion of the cell. With reference to Figure 3, the normal and tangential forces acting on a cut plane through the cell nucleus are (Bolander et al., 1999)

$$F_{n\theta} = \sum_i^N R_i [F_{ni} \cos(\pi - \alpha_i + \theta) + F_{ti} \sin(\alpha_i - \theta)] \quad (2)$$

$$F_{t\theta} = \sum_i^N R_i [F_{ni} \sin(\pi - \alpha_i - \theta) + F_{ti} \cos(\alpha_i + \theta)] \quad (3)$$

where N is the number of cell boundary segments. $R_i = a_i/b_i$ when boundary segment i intersects the cut plane; otherwise, R_i equals 1 or 0 depending on whether boundary segment i is entirely above or entirely below the cut plane, respectively. The normal and tangential stresses acting over the cut plane are

$$\sigma_\theta = F_{n\theta}/A_\theta \quad (4)$$

$$\tau_\theta = F_{t\theta}/A_\theta \quad (5)$$

where A_θ is the area of cross-sectional cut. The $(\sigma_\theta, \tau_\theta)$ pairs produced by varying θ from 0 to π form a Mohr's circle representation of the stress state at the cell nucleus. As shown later in this paper, and elsewhere (Bolander et al., 1999), stress maps produced from the RBSN are comparable in accuracy to those of constant strain triangle (CST) finite elements.

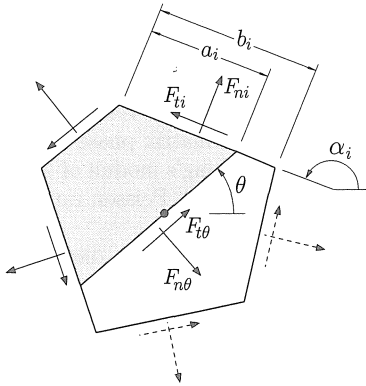


Figure 3. Force resultants acting on a section through the cell nucleus

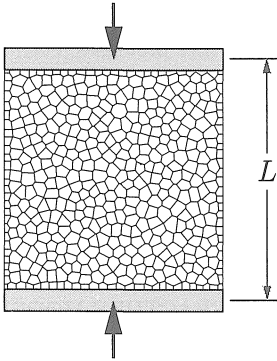


Figure 4. Homogeneous membrane structure under compressive loading

3.2 Elastic uniformity

The RBSN is elastically homogeneous under uniform straining (Bolander and Saito, 1998), as demonstrated by the following elastic analysis. Figure 4 shows a homogeneous membrane structure that is free of lateral restraint along the load platen surfaces. Imposing a vertical displacement, $-\delta$, on the top platen produces a uniform compressive strain of magnitude δ/L . Figure 5a shows the Mohr circle representation of stress at each of the 480 cell nuclei, as provided by the stress retrieval algorithm for $\theta = n\pi/90$ where $n = 1, \dots, 90$. No lateral tension is produced, in accordance with theory.

3.3 Modeling Poisson effect

To achieve elastic uniformity, the spring sets connecting the rigid cells must be isotropic (i.e. $k_t = k_n$, as shown in Eqs. 1). That being the case, however, the model exhibits no Poisson effect, as if Poisson ratio $\nu = 0$. Many important applications, such as the compressive response of heterogeneous

materials studied later in this paper, require an accurate modeling of Poisson effect.

By setting $k_t = \eta k_n$ for all spring sets, the coefficient η can be adjusted to achieve the desired macroscopic Poisson ratio (Kiyosue, 1995). For the network shown in Figure 4, $\eta = 0.35$ is required to achieve a macroscopic Poisson ratio of $\nu = 0.2$. For $\eta \neq 1$, however, the network is no longer elastically uniform, since the local stiffness is biased by facet orientation. The resulting scatter in stress values, shown in Figure 5b, can be regarded as spurious heterogeneity of the system. Moreover, a proper point-wise representation of ν is still missing. The following section introduces means for accurately modeling both global and local Poisson effect within the random lattice, without sacrificing its elastic homogeneity.

3.4 RBSN-FE hybrid approach

The basic idea is to overlay the RBSN with constant strain triangle (CST) finite elements arranged according to the Delaunay triangulation of the Voronoi nuclei (Fig. 6). The material

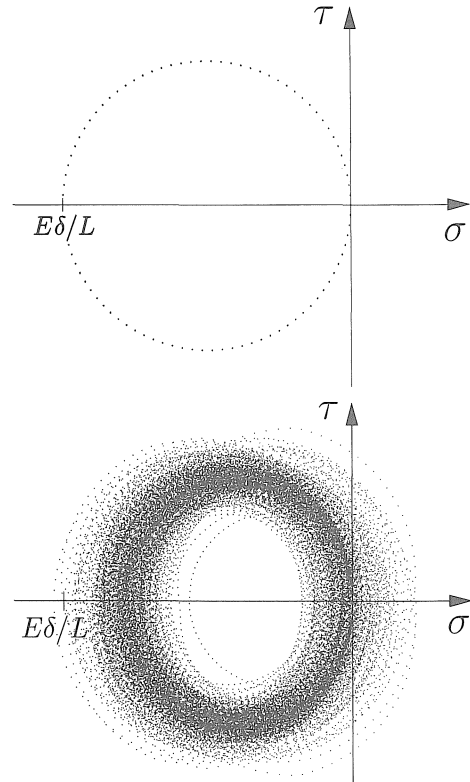


Figure 5. Mohr circle representation of stress at cell nuclei: a) RBSN model ($\eta = 1$); b) $\eta = 0.35$

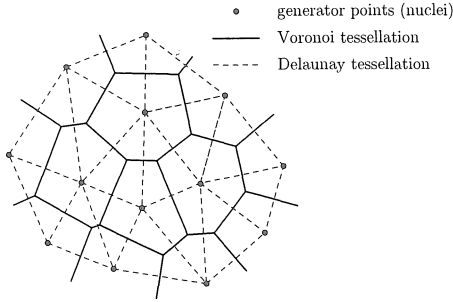


Figure 6. Dual tessellations of a set of generator points

relations for the CST elements are defined so that these elements only contribute Poisson effect to the network. That is, the RBSN (with $\nu = 0$) is overlaid with CST finite elements with the following material matrix:

$$\mathbf{C}^* = \mathbf{C}(E, \nu) - \mathbf{C}(E, \nu = 0) \quad (6)$$

where $\mathbf{C}(E, \nu)$ is the conventional material matrix used for plane stress analysis

$$\mathbf{C}(E, \nu) = \begin{bmatrix} \frac{E}{1-\nu^2} & \frac{\nu E}{1-\nu^2} & 0 \\ \frac{\nu E}{1-\nu^2} & \frac{E}{1-\nu^2} & 0 \\ 0 & 0 & \frac{E}{2(1+\nu)} \end{bmatrix} \quad (7)$$

By the principle of superposition, the result is a hybrid system that has the desired elastic properties. For $\nu = 0$, the overall formulation reverts to that of ordinary RBSN.

For the previous example shown in Figure 4, the vertical displacement $-\delta$ of the top platen produces a lateral strain of $\nu\delta/L$, both globally and in a local sense, as measured between the nuclei of contiguous cells. Stresses retrieved from the model also match theory, provided that the stresses from the CST elements are added to the stresses extracted from the RBSN. Since the CST stresses are determined within each element domain, simple averaging is used to determine the CST stress contributions at the cell nuclei. The spring network actually goes into lateral tension while the finite elements are in compression. The sum of the two lateral stress components is zero, in accordance with theory.

3.5 Stress analysis of heterogeneous systems

The utility of the RBSN hybrid approach is demonstrated in the following example. The Voronoi discretization, shown in Figure 7, is used to perform RBSN-FE and finite element stress analyses for a specimen with a single, centrally

located inclusion. For objective comparison, the CST elements are defined by the Delaunay tessellation of the Voronoi diagram nuclei. Here, too, we assume no lateral restraint along the loading surfaces. The matrix phase and inclusion phase are assigned Young's moduli of 20 GPa and 62.5 GPa, respectively. A Poisson ratio $\nu = 0.2$ is assigned to both phases.

The principal tensile stress distributions for the hybrid RBSN approach and the CST finite elements are similar, as shown in Figure 8. Higher tensile stresses appear to the sides of the inclusion, whereas for the case of $\nu = 0$ (Thomure, 2000), a higher tensile stress region forms above and below the inclusion. This suggests that Poisson ratio has a significant effect on the stress distribution, and possibly fracture processes, even though both phases have been assigned the same Poisson ratio. Due to the modular mismatch between the phases, accurate representation of Poisson effect is not a secondary issue in modeling the compression specimens, even though the Poisson ratios of the matrix and inclusions are similar.

4 OBJECTIVE FRACTURE MODEL

The ability to represent fracture objectively, with respect to average element size and network geometry, is a fundamental requirement of the fracture model. This requirement is realized by implementing a crack band model within the RBSN.

4.1 Crack band modeling of fracture

Figure 9 shows normal and tangential spring set forces for a two-cell assembly. For primarily tensile loadings, the crack band is assumed to form

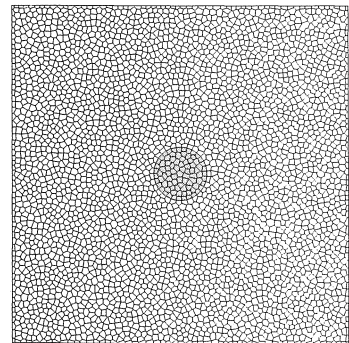


Figure 7. Voronoi cell discretization of membrane with circular inclusion

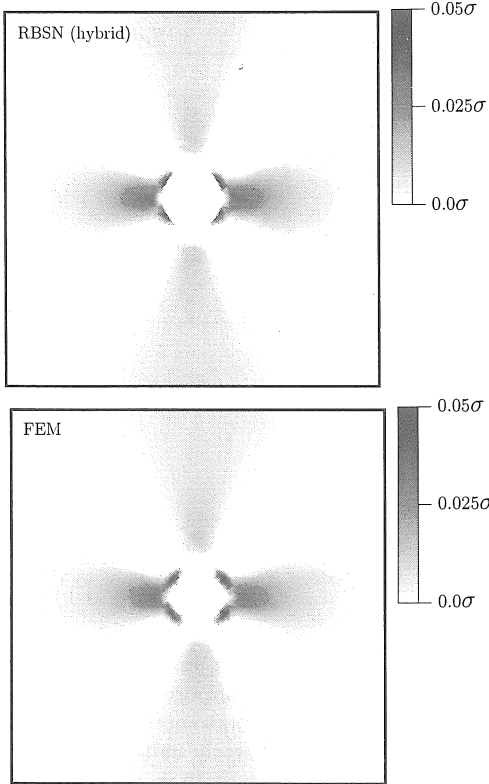


Figure 8. Stress contours for concrete specimen with one inclusion

perpendicular to the resultant of this force pair, F_R . The crack band width is $h \cos \theta_R$, which is the distance between the corresponding cell nuclei in the direction of F_R . The crack band length is $\ell \cos \theta_R$, where ℓ is the length of the common boundary segment. The average stress acting over the crack band is $\sigma_R = F_R / (t \ell \cos \theta_R)$, where t is the material thickness. Stress σ_R and a softening relation (as shown in Figure 10, for example) are then used to define the fracture criterion.

During each load step, the elastic properties of critical spring sets are degraded, in accordance with the softening relation, through a series of partial fracture events. One fracture event is permitted per computational cycle. To realize constant fracture energy consumption for different cell sizes, damage is assumed to be uniformly distributed over the element length according to the crack band concept of Bazant and Oh (1983). Strain values characterizing the softening response are dependent on crack band width

$$\epsilon^{cr} = \frac{w}{h \cos \theta_R} \quad (8)$$

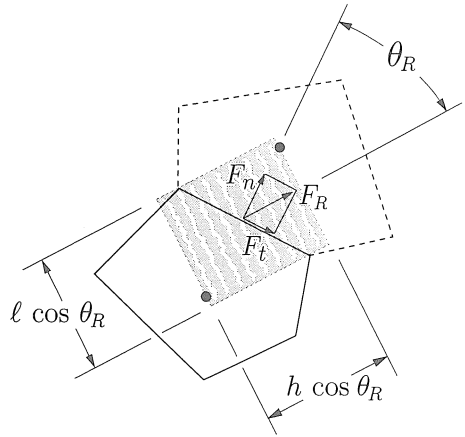


Figure 9. Crack band model for objective fracture criterion

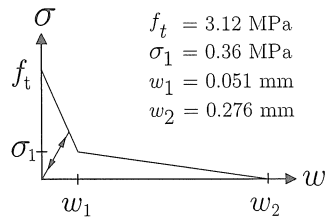


Figure 10. Bilinear softening diagram and parameters extracted from inverse analysis

where ϵ^{cr} is the crack strain and w is the crack opening displacement, as defined by the softening diagram.

4.2 Numerical analysis

Compact Tension (CT) fracture specimens tested by Wittmann et al. (1990) were first analyzed using a RBSN model with an embedded straight crack (Fig. 11a). The softening parameter values, indicated in Figure 10, were determined through an inverse analysis procedure, based on a Levenberg-Marquardt minimization algorithm (Thomure, 2000). With the derived parameter set, a forward analysis reproduces the experimental result, as shown in the Figure 12.

Using the same softening parameters, the analysis is repeated using the quasi-random discretization over the ligament length shown in Figure 11b. The load-displacement results agree well with those of the benchmark case. The reasons for this behavior can be explained by studying energy consumption along the crack trajectory.

An energy value is associated with each discrete fracture event by monitoring the change in reactive force at the load points under constant

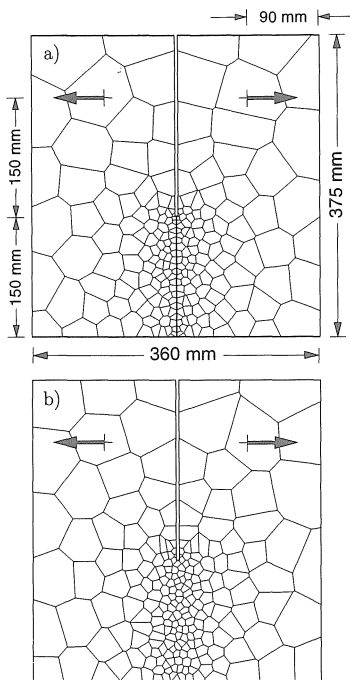


Figure 11. Mesh designs: a) straight line discretization along ligament length; b) random discretization along ligament length

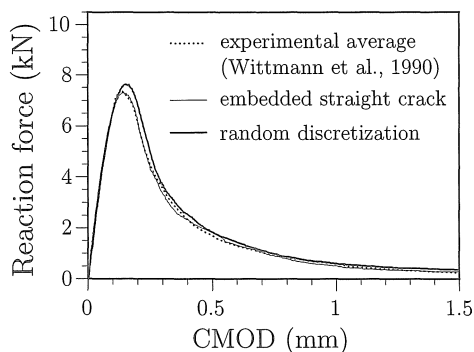


Figure 12. Load versus CMOD response

displacement. This information is stored and later retrieved in a post-processing module, so that the distribution of local energy consumption, g_F , can be viewed at any load stage. Figure 13 shows distributions of energy consumption (up through a load point displacement of 2.25 mm) for the straight crack and random crack geometries. Each segment of the energy distribution plot corresponds to a damaged spring set. The energies have been normalized by G_F , the area under the bilinear softening diagram (Fig. 10).

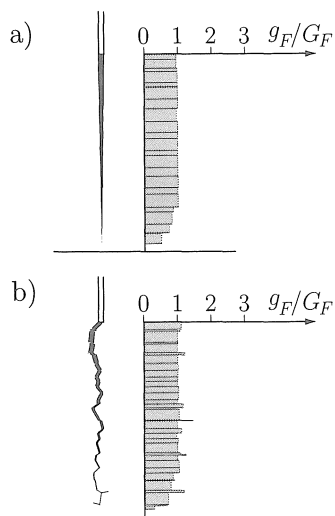


Figure 13. Fracture energy distributions along ligament length for: a) embedded straight crack path; b) random discretization

As expected, the straight crack analysis produces uniform energy consumption along the crack trajectory. For the random geometry analysis, the energy distributions are nearly uniform along the principal crack trajectory, with $g_F/G_F \approx 1.0$. Crack propagation through the random mesh produces nearly the same results as crack propagation along a smooth, predefined pathway. This is desirable in that network random geometry does not represent any structural features within the material.

5 COMPRESSIVE FAILURE OF MODEL CONCRETE SPECIMENS

As a first step toward modeling concrete compressive failure, the RBSN is being used to simulate failure in two-dimensional model concrete specimens tested by Choi and Shah (1999). The specimens consisted of a mortar matrix containing cylindric inclusions that extend through the specimen width, which was kept small to minimize three-dimensional effects. The specimens were subjected to uniaxial compression by displacement controlled loading, with minimal lateral restraint due to the load platen surfaces.

The specimen considered here contains one centrally located, stiff inclusion, similar to the arrangement analyzed in Section 3.5. The failure pattern observed during testing was measured

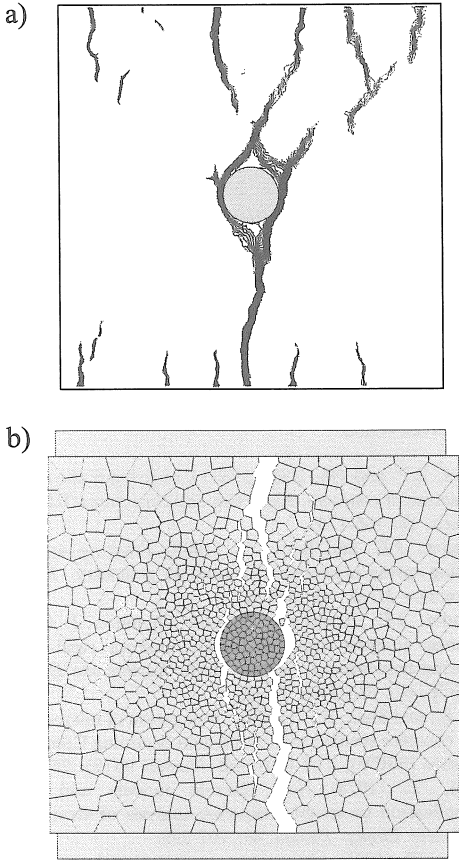


Figure 14. Vertical splitting of model concrete with one inclusion : a) localization of surface displacements measured during testing; b) RBSN simulation

using Subregion Scanning Computer Vision (Choi and Shah, 1999). The technique is based on Digital Image Correlation and provides high-resolution, full-field mappings of specimen surface displacements. Here, only the closely spaced contour lines, indicating surface displacement localization, are shown in Figure 14a.

The RBSN model now represents a three-phase composite consisting of a mortar matrix, an inclusion, and the matrix-inclusion interface. Figure 14b shows the failure pattern obtained using an earlier version of the RBSN. Fracture initiated along the weak interface and, even with simple breaking rules governing the fracture modeling, the numerical specimen exhibits a damage pattern similar to that witnessed during testing. Shear cones above and below hard inclusions have been observed within other experimental programs, as well (Stroeven, 1973, van Mier, 1984).

Concrete materials and fracture processes are three-dimensional (van Mier, 1997). Compressive failure is affected by the mechanical properties, spatial distribution, and volume fractions of the constituent phases, as well as the structural boundary conditions of the specimens considered. The preceding two-dimensional lattice networks are therefore applicable to only a small set of the current research needs in concrete modeling. Fortunately, apart from some of the challenging material modeling issues, there are few conceptual barriers to three-dimensional concrete modeling with RBSN. In fact, the Kawai RBSM approach has been used to simulate the three-dimensional behavior of brittle solids with microinclusions (Kiyosue, 1995). Foreseeable challenges include those associated with computing time and memory requirements for solving the large linear equation sets, as well as the pre/post-processing demands that accompany three-dimensional analysis.

Figure 15 shows a Voronoi discretization of a three-dimensional homogeneous body, free of redundant constraints. Elastic uniformity of the associated RBSN is studied by subjecting the body to a uniform temperature loading. Figure 16a shows the histogram of axial strain, ϵ , between each pair of contiguous cell nuclei within the domain, normalized by the temperature strain ϵ_t . All measured strains are equal to ϵ_t , indicating the abilities of RBSN for elastic stress analysis described in Section 3 are likely to be valid for the three-dimensional setting, as well. If the network degrees of freedom are defined at the cell volume centroids, rather than at the nuclei, then the temperature loading produces spurious straining throughout the network, as shown by Figure 16b.

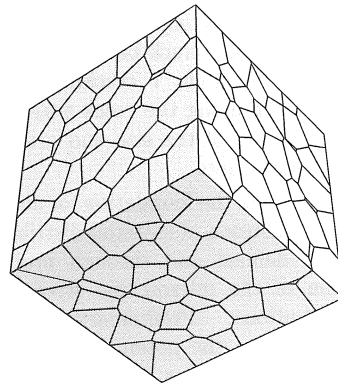


Figure 15. Three-dimensional Voronoi diagram (320 cells)

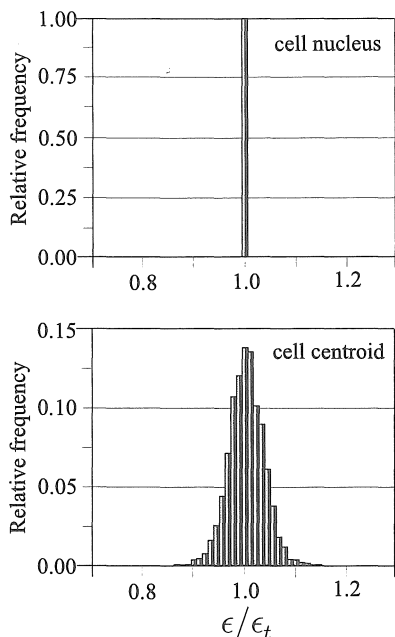


Figure 16. Strain production in thermally loaded three-dimensional networks: a) RBSN; b) network degrees of freedom defined at cell volume centroids

7 CONCLUSION

This paper overviews recent development of the Rigid-Body-Spring Network approach and its application to modeling fracture in cement-based composites. Attention has been given to accurate modeling of the elastic properties of both homogeneous and heterogeneous media. In particular, a hybrid approach has been developed, which involves finite element technology to embed a controllable Poisson effect within the RBSN, without sacrificing elastic uniformity of the network. An objective means of modeling fracture is based on the implementation of a crack band model within the RBSN. During mode I cracking, fracture energy consumption along the crack trajectory is uniform, independent of the size and orientation of the lattice components.

This work provides the foundation for analyzing more complex loadings and material distributions, both explicitly defined and through probabilistic description of the microscopic strength and stiffness distributions. Preliminary work, presented here, indicates the potential of RBSN for identifying and interpreting the mechanisms of compressive failure in cement-based composites.

Ultimately, a three-dimensional description of the material and failure process is necessary. As a first step in this direction, this paper has demonstrated elastic uniformity of a three-dimensional RBSN under uniform thermal loading.

ACKNOWLEDGEMENT

The authors would like to thank Mr. John Lawler at the Center for ACBM, Northwestern University, for his contributions to this work.

REFERENCES

- Bazant, Z.P. and Oh, B.H. (1983) Crack band theory for fracture of concrete, *Materials and Structures*, RILEM, Paris, 16: 155-176.
- Bolander, J.E. and Saito, S. (1998) Fracture analysis using spring networks with random geometry. *Engng. Fracture Mech.*, 61: 569-91.
- Bolander, J.E., Yoshitake, K. and Thomure, J. (1999) Stress analysis using elastically uniform rigid-body-spring networks, *J. Struct. Mech. Earthquake Engng.*, JSCE, No. 633/I-49: 25-32.
- Choi, S., and Shah, S.P. (1999) Propagation of microcracks in concrete studied with Subregion Scanning Computer Vision (SSCV), *ACI Materials Journal*, 96 (2): 255-269.
- Kawai, T. (1978) New discrete models and their application to seismic response analysis of structures. *Nuclear Engng. Design*, 48: 207-229.
- Kiyosue, T. (1995) Mesoscopic computational mechanics of brittle solids containing microinclusions, Doctoral dissertation, University of Tokyo, Japan. (in Japanese)
- van Mier, J.G.M. (1984) Strain softening of concrete under multiaxial loading conditions. Ph.D. thesis, Eindhoven University of Technology, The Netherlands.
- van Mier, J.G.M. (1997) *Fracture Processes of Concrete*, CRC Press, Boca Raton, Florida, 448 pp.
- Schlängen, E. (1995) Computational aspects of fracture simulations with lattice models, In *Fracture Mechanics of Concrete Structures*, Ed. F.H. Wittmann, Aedificatio Publishers, Freiburg, Germany, pp. 913-928.
- Schlängen, E. and van Mier, J.G.M. (1992) Experimental and numerical analysis of micromechanisms of fracture of cement-based composites, *Cem. Conc. Composites*, 14: 105-118.
- Stroeven, P. (1973) Some aspects of the micromechanics of concrete, Ph.D. thesis, Delft University of Technology, The Netherlands.
- Thomure, J.L. (2000) Simulating tensile and compressive failure in concrete materials, M.S. degree thesis, Dept. Civil & Environmental Engineering, University of California, Davis.
- Wittmann, F.H., Mihashi, H. and Nomura, N. (1990) Size effect on fracture energy of concrete, *Engng. Fracture Mechanics*, 35 (1/2/3): 107-115.